JACS
JOURNAL OF THE AMERICAN CHEMICAL SOCIETY

ARTICLE

pubs.acs.org/JACS

The Nature of In-Plane Skeleton Raman Modes of P3HT and Their Correlation to the Degree of Molecular Order in P3HT:PCBM Blend Thin Films

Wing C. Tsoi,[†,‡] David T. James,[†] Jong Soo Kim,[†] Patrick G. Nicholson,[‡] Craig E. Murphy,[*,‡] Donal D. C. Bradley,[†] Jenny Nelson,[†] and Ji-Seon Kim[*,†,§]

[†]Department of Physics and Centre for Plastic Electronics, Imperial College London, London SW7 2AZ, United Kingdom

[‡]National Physical Laboratory (NPL), Teddington, Middlesex TW11 0LW, United Kingdom

[§]Department of Materials Science and Engineering, KAIST, Daejeon 305-701, Republic of Korea

Supporting Information

ABSTRACT: The nature of main in-plane skeleton Raman modes (C═C and C−C stretch) of poly(3-hexylthiophene) (P3HT) in pristine and its blend thin films with [6,6]-phenyl-C_{61}-butyric acid methyl ester (PCBM) is studied by resonant and nonresonant Raman spectroscopy and Raman simulations. Under resonant conditions, the ordered phase of P3HT with respect to its disordered phase is identified by (a) a large shift in the C═C mode peak position to lower wavenumber (∼21 cm^{-1} shift), (b) a narrower fwhm of the C═C mode (∼9 cm^{-1} narrower), (c) a larger intensity of the C−C mode relative to the C═C mode (∼56% larger), and (d) a very small Raman dispersion (∼5 cm^{-1}) of the C═C mode. The behavior of the C═C and C−C modes of the ordered and disordered phases of P3HT can be explained in terms of different molecular conformations. The C═C mode of P3HT in P3HT:PCBM blend films can be reproduced by simple superposition of the two peaks observed in different phases of P3HT (ordered and disordered). We quantify the molecular order of P3HT after blending with PCBM and the subsequent thermal annealing to be 42 ± 5% and 94 ± 5% in terms of the fraction of ordered P3HT phase, respectively. The increased molecular order of P3HT in blends upon annealing correlates well with enhanced device performance (J_{SC}, −4.79 to −8.72 mA/cm^2 and PCE, 1.07% to 3.39%). We demonstrate that Raman spectroscopy (particularly under resonant conditions) is a simple and powerful technique to study molecular order of conjugated polymers and their blend films.

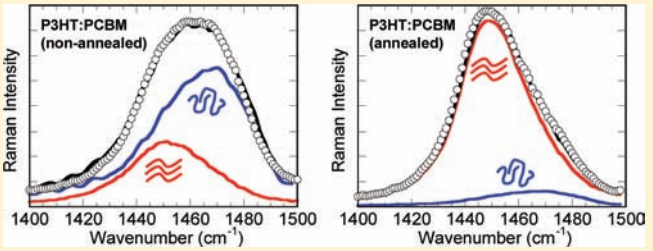

INTRODUCTION

Ordering of molecules in semiconducting polymeric materials can have significant effects on their optoelectronic properties. For example, thin films of regioregular poly(3-hexylthiophene) (RR-P3HT) can exhibit a high degree of molecular order ($\pi-\pi$ stacking of molecules).[1] This high degree of molecular order can lead to an increase in absorption at longer wavelength and a dramatic increase in charge carrier mobility as compared to its disordered form.[2−4] Therefore, understanding of this molecular order is important to clarify the structure−property relationship in RR-P3HT thin films and to make use of these thin films as active layers in various optoelectronic devices. An application of particular interest is the use of RR-P3HT as the light absorbing and hole transporting component in solar cells fabricated from RR-P3HT blended with [6,6]-phenyl C_{61} butyric acid methyl ester (PCBM).[5−7] In RR-P3HT:PCBM blend films, the order in packing of RR-P3HT molecules is largely disturbed by PCBM molecules. Post deposition treatments of these blend films such as thermal annealing, however, restore the order of RR-P3HT molecules, leading to an increase in both absorption at longer wavelength and charge carrier mobility, and thus producing a significant increase in power conversion efficiency of the photovoltaic devices.[8−10]

Raman spectroscopy is a simple, widely used technique to study vibrational modes of molecules. This technique together with quantum-chemical calculations of Raman modes can provide an important insight into the fundamental structure−property relationships of molecular materials.[11−13] In particular, surface-enhanced Raman spectroscopy provides a basis to study vibrational modes of molecules down to the single molecular level,[14,15] and the development of tip-enhanced Raman spectroscopy has the promising potential to map chemical compositions of organic blend films at the nanometer scale.[16,17] Furthermore, Raman spectroscopy is a nondestructive technique, which can be used to monitor the conformational changes of molecules in situ, for example, during processing treatments such as annealing or during operation of a device.[18−21] Studies of semiconducting polymeric materials with Raman spectroscopy are usually performed in nonresonant conditions (i.e., molecules

Received: February 11, 2011
Published: May 26, 2011

are excited by an incident energy lower than their optical band gaps) to avoid direct electronic excitation, which can produce strong fluorescence background and therefore may cover weak Raman signals. Raman spectroscopy in resonant conditions (i.e., when the Raman excitation wavelength is close to the absorption maximum of molecules), on the other hand, has the potential of providing deeper insight into the understanding of molecular structures, for example, by selectively exciting different phases in blend systems, and associated electron−phonon coupling.[22,23] A weak Raman signal can also be significantly enhanced by resonant effect, once fluorescence background is shifted away from the vibrational energy range with properly chosen excitation energy.[22,23]

Raman spectroscopy has been used to study RR-P3HT and its blend with PCBM (before and after thermal or solvent annealing) at a specific excitation wavelength.[17,24−27] It has been reported that under nonresonant and preresonant excitation conditions (e.g., excitation at 785 and 633 nm), thermal or solvent annealing of RR-P3HT:PCBM thin films, which increases the ordering of P3HT molecules, causes a reduction in the full-width-half-maximum (fwhm) of the P3HT symmetric C═C stretching mode (∼1445 cm^{-1}) without any observable changes in its peak position.[17,24] However, under resonant excitation conditions (e.g., excitation at 514, 488, or 496.5 nm), annealing induces a significant shift of the peak position of the C═C mode to lower wavenumber.[25−27] On the other hand, nonannealed RR-P3HT:PCBM thin films show a shift in the peak position of this C═C mode to higher wavenumber with increasing excitation energy.[25−27] Despite these interesting observations, there has been no fundamental discussion about the effects and thus the reliability and potential of using Raman spectroscopy as a tool to distinguish different phases of the molecules.

In this Article, we aim to understand the nature of the C═C Raman mode of P3HT with a particular focus on its behavior under different excitation wavelengths (resonant, nonresonant, and preresonant conditions). For this study, we use disordered regiorandom P3HT (RRa-P3HT) as a reference material and compare it to ordered regioregular P3HT (RR-P3HT). In particular, we compare the C═C Raman mode in RRa-P3HT and RR-P3HT films to the respective blend films with PCBM before and after annealing. We find that the C═C mode of RR-P3HT in RR-P3HT:PCBM films (both nonannealed and annealed) observed under all excitation wavelengths used (785, 633, 514, 488, and 457 nm) can be explained in terms of a simple superposition of the C═C modes characteristic of the ordered and disordered phases of P3HT. On the basis of this observation, we discuss how analysis of the C═C mode can be used as a tool to quantify the degree of molecular order of P3HT in the blend films. We also perform Raman simulations to show the correlation between the different behavior of the C═C and C−C modes in ordered and disordered P3HT phases to their different molecular conformations. The degree of molecular order of P3HT in the blend films is well correlated with the performance of the corresponding solar cells.

EXPERIMENTAL SECTION

Film Preparation. Regiorandom P3HT (RRa-P3HT) (regioregularity = 1:1 (head-to-head):(head-to-tail) linkages of regioisomers) was purchased from Aldrich. The weight-average molecular weight (M_w) is ∼87 kg/mol. Regioregular P3HT (RR-P3HT) was synthesized by Merck Chemicals. The weight-average (M_w) and number-average (M_n) molecular weights, polydispersity index, and regioregularity are 54.2 kg/mol, 23.6 kg/mol, 2.29 and 94.2%, respectively. PCBM was purchased from API Service, Inc. All of the materials were used as received. For pristine films, 25 mg of each RRa-P3HT, RR-P3HT, and PCBM were dissolved in 1 mL of chlorobenzene solvent. The solutions were then spin-coated on glass substrates at 1500 rpm for 60 s. For blend films, 25 mg of RRa-P3HT (or RR-P3HT) and 25 mg of PCBM were mixed in chlorobenzene solvent and warmed at ∼60 °C (with stirring) overnight to fully dissolve the materials. The solutions were then spin-coated on glass substrates at 1500 rpm for 60 s. The films were annealed at 140 °C for 30 min inside a nitrogen glovebox. Thicknesses of the films are pristine RRa-P3HT ∼80 nm, pristine RR-P3HT ∼80 nm, pristine PCBM ∼50 nm, RRa-P3HT:PCBM ∼150 nm, and RR-P3HT:PCBM ∼150 nm. The thicknesses were measured with an atomic force microscope (Ntegra probe laboratory, NT-MDT).

Absorption Measurements. Absorption spectra were recorded using a UV−vis spectrophotometer (UV-2550, Shimadzu).

Raman Measurements. Raman spectra were recorded at five different excitation wavelengths, 785, 633, 514, 488, and 457 nm (50× objective) with a Renishaw inVia Raman microscope in a back scattering configuration. The excitation conditions were as follows. At 785 nm, 0.93−1.86 mW and acquisition time of 10−60 s; at 633 nm, 0.1−0.5 mW and acquisition time of 1−10 s; at 514 and 488 nm, 0.01 mW and acquisition time of 10−20 s; at 457 nm, 18 μW and acquisition time of 20 s. For 514, 488, and 457 nm excitations (resonant excitations), the laser beam was defocused to a beam diameter of ∼8 μm to avoid photodegradation of the samples. The Raman spectra were background corrected and obtained by averaging the spectra obtained at three different regions in the sample. The spectra at the different regions are very similar, demonstrating the reproducibility of the results. The spectral resolution is ∼1 cm^{-1}.

Raman Simulations. Raman spectra of thiophene oligomers were calculated using density functional theory (DFT) at the B3LYP/6-31G* level of theory within the Gaussian 09 package.[28] The calculations were done under nonresonant conditions. In each case, the ground-state geometries of the molecules were first optimized in the gas phase (in the calculations, the hexyl side chains attached to the conjugated backbone were replaced by hydrogen atoms) and the Raman spectra of these optimized structures were then calculated. The effect of increasing oligomer length on the vibrational modes was investigated by calculating the Raman spectra of the geometrically optimized thiophene molecules with unit from 3 to 7. The effect of polymer backbone planarity on the vibrational modes was investigated by calculating Raman spectra of the thiophene oligomer of length seven in both helical and alternative structures with dihedral angles varying from 0° to 40° (see Figure 6 for the structures). This range of dihedral angles has been used for oligothiophenes.[29] At a fixed dihedral angle between thiophene units, the geometry of the molecule was reoptimized prior to calculating its Raman modes. The use of nonsubstituted oligomers appears to us as a reasonable compromise between the computational requirements and the need for a reasonable (albeit imperfect) description for the alkylthiophene polymers.

Device Fabrication and Characterization. Indium tin oxide (ITO)-coated glasses were used as the substrates. After the ITO-coated glasses were cleaned with detergent (Mucasol), acetone, and isopropyl alcohol, ∼30 nm thick poly(3,4-ethylenedioxythiophene)-poly(styrene sulfonate) (PEDOT-PSS, Baytron P TP AI 4083, Bayer AG) layer was spin coated on top of the substrates. The PEDOT:PSS/ITO coated glasses were then annealed at 120 °C for 30 min. RRa-P3HT:PCBM and RR-P3HT:PCBM (both in 1:1 by weight ratio) were dissolved in chlorobenzene and stirred overnight. The solutions were spin coated on top of the PEDOT:PSS layer with a thickness of ∼120 nm. The films were then thermal annealed at 150 °C for 20 min. Ca (20 nm)/Al (80 nm) were then thermally evaporated on top of the films. The power conversion efficiencies and the corresponding device parameters of

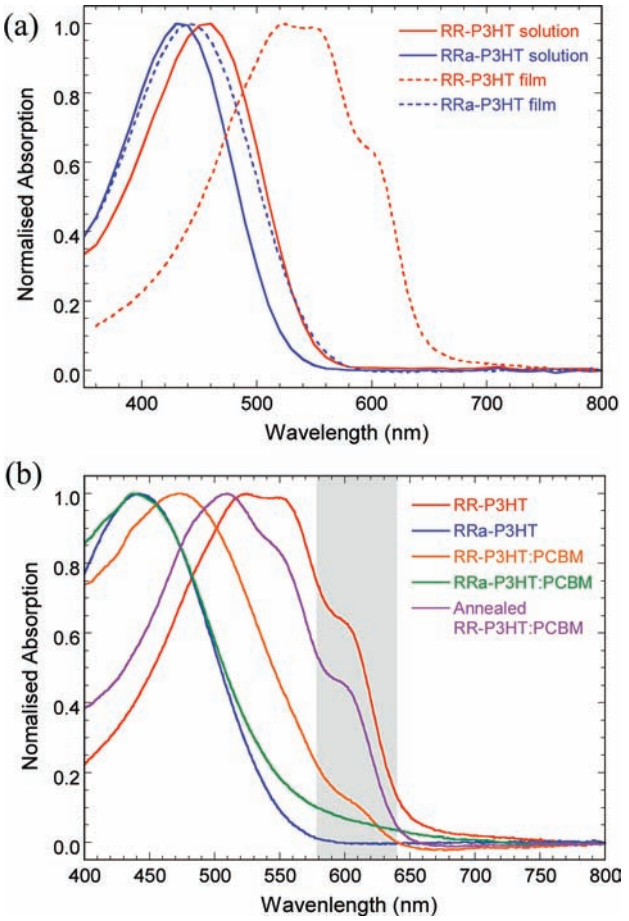

Figure 1. (a) Optical absorption spectra of RR-P3HT and RRa-P3HT in thin films and in dilute solutions, respectively. (b) Optical absorption spectra of RR-P3HT, RRa-P3HT, RR-P3HT:PCBM, RRa-P3HT:PCBM, and annealed RR-P3HT:PCBM thin films.

the solar cells were measured inside a nitrogen filled chamber at 100 mW/cm^2 under AM 1.5 conditions.

RESULTS AND DISCUSSION

Absorption Spectra of Films. Optical absorption spectroscopy is first used to identify the ordering of P3HT molecules; that is, the ordered P3HT shows a significant absorption shoulder at ~600 nm. By using this technique, we first study the degree of ordering of P3HT molecules in thin films and in nonannealed and annealed blend films with PCBM. The Raman data obtained later are then compared to these absorption data to better understand the changes in the phase of P3HT molecules from more disordered to ordered forms and vice versa. We also use the absorption spectrum of P3HT to determine the resonant, nonresonant, and preresonant conditions for Raman measurements.

RRa-P3HT film has been found to be amorphous with no measurable X-ray diffraction (XRD) peaks.[30] By comparing the absorption spectra of RRa-P3HT and RR-P3HT in dilute solutions (0.001 wt %), we observed that the absorption features from the less ordered phase of RR-P3HT in dilute solutions are very similar to those obtained from amorphous RRa-P3HT in thin films (Figure 1a). This can be understood from the fact that in dilute solutions, the RR-P3HT molecules are well

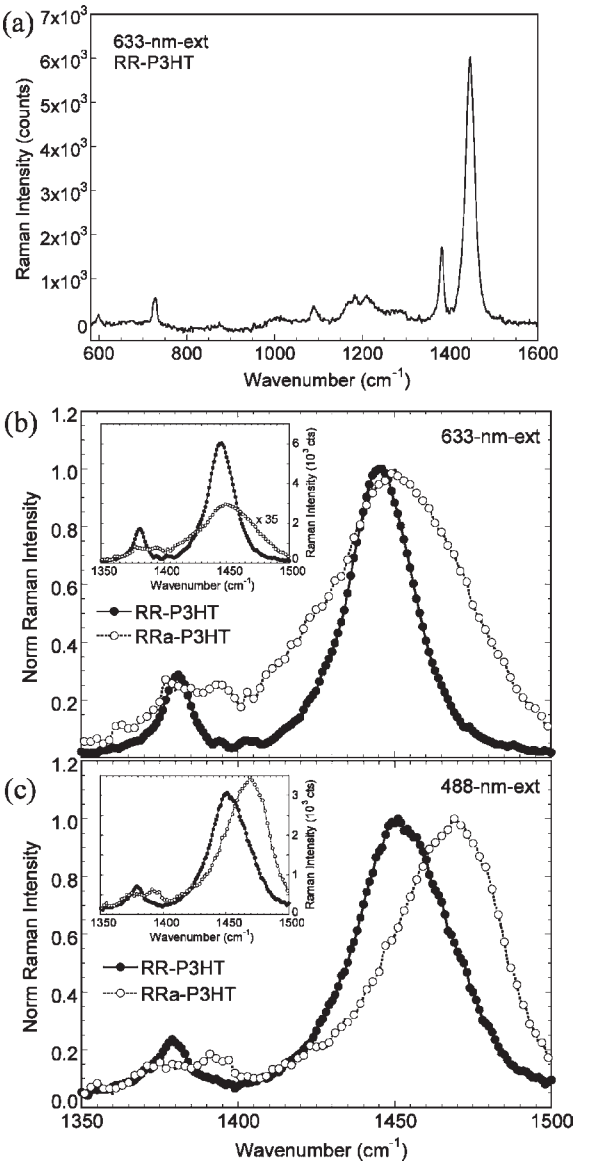

Figure 2. (a) Raman spectrum of RR-P3HT thin film under 633 nm excitation. (b) Normalized Raman spectra (C═C and C−C modes) of RR-P3HT and RRa-P3HT thin films under 633 nm excitation. The raw spectra are shown in the inset. The intensity of the Raman spectrum of RRa-P3HT thin film is magnified by 35 times for better visualization. (c) Normalized Raman spectra (C═C and C−C modes) of RR-P3HT and RRa-P3HT thin films under 488 nm excitation. The raw spectra (not magnified) are shown in the inset.

separated from each other without any measurable long-range order, so that they produce absorption features similar to disordered RRa-P3HT films. The pristine RR-P3HT film shows a strong absorption shoulder at ~600 nm, indicating the ordered phase, which is absent in the RRa-P3HT film (Figure 1a and b). The absorption spectra of RRa-P3HT and RR-P3HT films after thermal annealing are very similar to those before annealing (see the Supporting Information). After blending with PCBM molecules, the RRa-P3HT does not show any significant changes in its thin-film absorption spectrum, while the RR-P3HT shows noticeable changes in the absorption spectrum with a largely reduced intensity at ~600 nm due to the increase in disorder in

dx.doi.org/10.1021/ja2013104 |J. Am. Chem. Soc. 2011, 133, 9834–9843

P3HT chain packing induced by PCBM molecules (Figure 1b). After annealing the RRa-P3HT:PCBM blend film, again there is no measurable change in the absorption spectrum (data not shown), while for the RR-P3HT:PCBM blend film, we observed a significant increase in the absorption intensity at ~600 nm due to the restored molecular order of P3HT upon annealing (Figure 1b).

Raman Spectra of Pristine Films. Figure 2a shows a typical Raman spectrum of RR-P3HT thin film excited at 633 nm. There are various Raman modes at 600−1600 cm^{-1}:[31,32] the main in-plane ring skeleton modes at ~1445 cm^{-1} (symmetric C═C stretch mode) and at ~1381 cm^{-1} (C−C intraring stretch mode), the inter-ring C−C stretch mode at ~1208 cm^{-1}, the C−H bending mode with the C−C inter-ring stretch mode at ~1180 cm^{-1}, and the C−S−C deformation mode at 728 cm^{-1}. Among these Raman modes, we focus on the two main in-plane ring skeleton modes at ~1445 and ~1381 cm^{-1}, as they are supposed to be sensitive to π-electron delocalization (conjugation length) of P3HT molecules.[23,26]

Figure 2b and c shows these two Raman modes of pristine RRa-P3HT and RR-P3HT films under 633 and 488 nm excitation, respectively. Under 633 nm excitation (Figure 2b), the Raman signal of the C═C mode of RR-P3HT film is much larger (~60−80 times more) than that of the RRa-P3HT film (Figure 2b, inset). This is due to the fact that RR-P3HT film has some absorption at 633 nm, which induces a preresonant Raman effect leading to an increase in the intensity of the Raman peaks. In contrast, RRa-P3HT film has almost no absorption at 633 nm (see Figure 1a). Figure 2b shows the corresponding normalized Raman spectra of the RR-P3HT and RRa-P3HT films. The peak position of the C═C mode is shifted to higher wavenumber from ~1445 cm^{-1} for RR-P3HT film to ~1450 cm^{-1} for RRa-P3HT film. Note that there is a large uncertainty in the peak position (±6 cm^{-1}) for RRa-P3HT film due to very small Raman signals of the RRa-P3HT film under 633 nm excitation. The fwhm of this C═C mode for RR-P3HT film (~24 cm^{-1}) is much smaller than that of RRa-P3HT film (~52 cm^{-1}), reflecting the higher degree of molecular order of P3HT in RR-P3HT film. On the other hand, the peak position of the C−C mode (~1381 cm^{-1}) is very similar for both RR-P3HT and RRa-P3HT films, while the intensity of the C−C mode relative to the C═C mode is ~0.10 ± 0.01 and 0.15 ± 0.01 for RRa-P3HT and RR-P3HT films, respectively. The relative intensities are calculated by integrating the peak areas of the C−C and C═C modes, and the uncertainty is estimated by average the $I_{C-C}/I_{C=C}$ values obtained at various positions in the sample. For RRa-P3HT film, which has double peaks at around the position of the C−C mode, we fit the double peaks with two Lorentzian components and used the integrated area of the Raman component peak at ~1381 cm^{-1} to calculate the intensity of C−C mode for direct comparison.

Under resonant excitation (488 nm) (Figure 2c), at which both RRa-P3HT and RR-P3HT films show comparable absorption features, the Raman intensity of the C═C mode of RRa-P3HT film is significantly enhanced and becomes similar to that of RR-P3HT film (Figure 2c, inset). This C═C mode of RRa-P3HT film shows a large shift to higher wavenumber (~20 cm^{-1}) in the maximum peak position (shifting from ~1450 to ~1470 cm^{-1}) and a much narrower fwhm (~41 vs ~52 cm^{-1}) as compared to the case for preresonant excitation. In contrast, there is only a small shift to higher wavenumber (~4 cm^{-1}) of this peak in RR-P3HT film (~1449 vs ~1445 cm^{-1}) with an increased fwhm

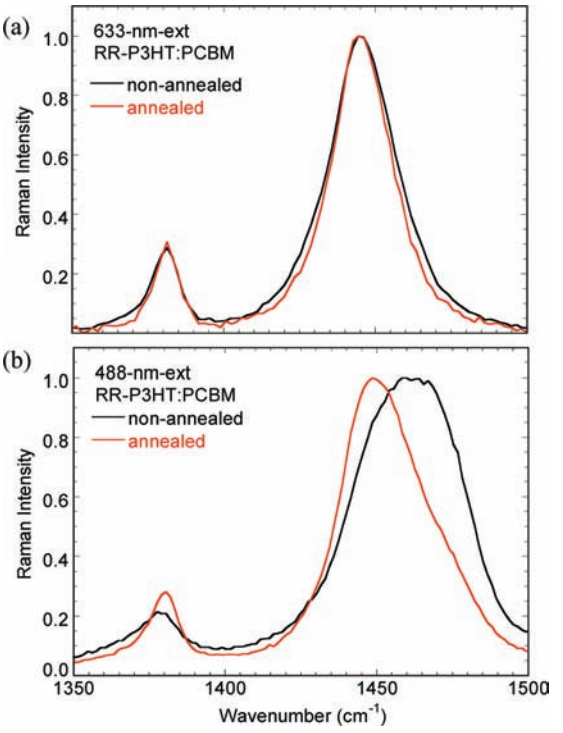

Figure 3. (a) Raman spectra (C═C and C−C modes) of nonannealed and annealed RR-P3HT:PCBM thin films under 633 nm excitation. (b) Raman spectra (C═C and C−C modes) of nonannealed and annealed RR-P3HT:PCBM thin films under 488 nm excitation.

(~32 vs ~24 cm^{-1}) when we compare excitation at 488 and at 633 nm (compare Figure 2c with b). Under 488 nm excitation, the Raman intensity of the C−C mode (~1380 cm^{-1}) relative to the C═C mode for RR-P3HT film is larger than that of the RRa-P3HT film ($I_{C-C}/I_{C=C}$ ~0.14 ± 0.01 versus ~0.09 ± 0.01). We notice that the peak position of the C−C mode with 488 nm excitation is similar to that with 633 nm excitation for both P3HT materials, which implies that the peak position of C−C mode is insensitive not only to the degree of molecular order, but also to the excitation wavelength. Annealing of both RRa-P3HT and RR-P3HT films did not induce any significant changes in their Raman spectra (data not shown).

Raman Spectra of Blend Films. We will now move on to the Raman spectra of the RR-P3HT:PCBM blend thin films before and after thermal annealing measured under preresonant (633 nm) and resonant (488 nm) excitation conditions. We note that under 633 nm excitation, the ordered phase of P3HT is under preresonant or even resonant condition as it has some absorption at this wavelength (Figure 1a), while the disordered phase of P3HT is under nonresonant as there is undetectable absorption at this wavelength (Figure 1a). On the basis of the Raman spectra of both RR-P3HT (ordered) and RRa-P3HT (disordered) pristine films with a particular focus on the nature of the C═C Raman mode, we attempt to understand different degrees of molecular order of P3HT induced in blend and upon subsequent thermal annealing.

Figure 3a shows the Raman spectra of RR-P3HT:PCBM blend film before and after thermal annealing under 633 nm excitation. We observed the Raman peak of the P3HT C═C mode in the RR-P3HT:PCBM blend film at the same position (~1445 cm^{-1}) as found in the pristine RR-P3HT film (compare with Figure 2b).

dx.doi.org/10.1021/ja2013104 |J. Am. Chem. Soc. 2011, 133, 9834–9843

Because this C=C peak position is sensitive to the degree of molecular order of P3HT (~1445 cm^{-1} for RR-P3HT and ~1450 cm^{-1} for RRa-P3HT), our data tend to indicate that there already existed some degree of order of P3HT molecules even in the nonannealed RR-P3HT:PCBM blend film. As the Raman intensity of the C=C mode measured in more ordered P3HT is ~60−80 times stronger than that measured in more disordered P3HT under 633 nm excitation, the Raman signal of C=C mode measured in the nonannealed blend film will be dominated by any ordered phases present in this film. This observation is consistent with the usually observed absorption feature at ~600 nm (ordered phase) even in the nonannealed RR-P3HT:PCBM blend films. Using electron diffraction measurements, it was found previously that nonannealed RR-P3HT:PCBM film exhibits some degree of P3HT crystallinity.[33] The fwhm of RR-P3HT:PCBM blend film under 633 nm excitation is ~26 cm^{-1}, which is slightly larger than that of the pristine RR-P3HT film (~24 cm^{-1}), implying more disordered P3HT in the blend film. Note that no Raman modes of PCBM molecules were observed under 633 nm excitation.

After annealing the RR-P3HT:PCBM blend film, the Raman intensity of the C=C mode under 633 nm excitation is increased approximately 3-fold (data not shown), which is well correlated with stronger absorption at ~600 nm induced by the more ordered P3HT upon annealing (Figure 1b). The Raman peak of the C=C mode in the annealed blend film under 633 nm excitation (Figure 3a) has the same position as that of nonannealed blend and pristine RR-P3HT films. The fwhm of the C=C mode in the blend film is reduced by ~3 cm^{-1} (from 26 to 23 cm^{-1}) after thermal annealing (Figure 3a), implying better molecular order of P3HT in the annealed film. Here and after, the Raman spectra were measured within the homogeneous region of the annealed blend films (i.e., away from the micrometer-sized PCBM aggregates, which are usually present after thermal annealing).

Under 633 nm excitation, there are no significant changes in the peak position and fwhm of the C−C mode when RR-P3HT is blended with PCBM and when the blend film is annealed (Figure 3a) due to the insensitivity of the peak position and fwhm of C−C mode to molecular order of P3HT under 633 nm excitation. On the other hand, the intensity of the C−C mode relative to the C=C mode is ~0.15 ± 0.01 for the nonannealed RR-P3HT:PCBM film, which is the same as that of the pristine RR-P3HT film and larger than that of the pristine RRa-P3HT film. This result can be explained by the preresonant or even resonant effect of the ordered phase of P3HT (RR-P3HT) under 633 nm excitation, dominating the intensity of the C−C and C=C modes. There is no considerable effect to the $I_{C-C}/I_{C=C}$ after thermal annealing. For RRa-P3HT, neither blending with PCBM nor annealing of the blend film leads to any significant changes in the Raman spectra at 633 nm excitation. Only the fluorescence background originating from RRa-P3HT is significantly changed, with the blends showing a dramatically reduced fluorescence background induced by blended PCBM molecules.

On the other hand, under resonant excitation (488 nm) (Figure 3b), the peak position of the C=C mode in the nonannealed RR-P3HT:PCBM blend film (~1460 cm^{-1}) lies between that of the RR-P3HT (~1449 cm^{-1}) and the RRa-P3HT pristine films (~1470 cm^{-1}). This observation indicates that the P3HT molecules in the nonannealed RR-P3HT:PCBM blend film, although being less ordered than that in the pristine RR-P3HT film, still contain some degree of molecular order as compared to the largely disordered RRa-P3HT film. The fwhm of the C=C peak of the nonannealed RR-P3HT:PCBM blend film is much broader than that under 633 nm excitation (43 versus 26 cm^{-1} (Figure 3b vs a)), indicating the possible existence of two components.

After annealing the RR-P3HT:PCBM blend film (Figure 3b), the peak position of C=C mode significantly shifts to lower wavenumber from ~1460 to ~1449 cm^{-1} due to a relatively strong reduction in the high-energy part of this peak. This reduction also leads to a significant decrease in fwhm of the C=C mode from 43 to 33 cm^{-1}. Such changes in the peak position and fwhm of the C=C mode resemble the differences in C=C peak position and fwhm between ordered and disordered P3HT phases under resonant conditions, that is, ~1449 cm^{-1} (32 cm^{-1}) for ordered RR-P3HT and ~1470 cm^{-1} (41 cm^{-1}) for disordered RRa-P3HT (Figure 2c), thus directly reflecting the enhanced degree of molecular order of P3HT in RR-P3HT:PCBM blend film upon annealing.

Under 488 nm excitation (Figure 3b), the Raman peak position of the C−C mode in the nonannealed RR-P3HT:PCBM blend film remains similar to that of the pristine RR-P3HT film, but with lower intensity relative to the C=C mode (0.12 ± 0.01 vs 0.14 ± 0.01 of pristine RR-P3HT film) and larger fwhm. The larger fwhm observed may originate from the possible double Raman C−C peaks appearing in disordered phase of P3HT, as observed in RRa-P3HT film (Figure 2c). Upon annealing, the peak position of the C−C mode of the RR-P3HT:PCBM film does not change much (only ~1 cm^{-1} shift to higher wavenumber), but its intensity relative to the C=C mode increases from 0.12 ± 0.01 to 0.14 ± 0.01 and its fwhm decreases, resembling the differences in C−C peak position, the $I_{C-C}/I_{C=C}$ ratio, and fwhm between ordered and disordered P3HT phases under resonant conditions (Figure 2c). These observations also support the change in phase of P3HT from more disordered in nonannealed blend films to more ordered in annealed blend films. For RRa-P3HT, blending with PCBM molecules or annealing of the RRa-P3HT:PCBM film does not induce any significant changes in their Raman spectra under 488 nm excitation (data not shown).

These significantly different characteristics of the main in-plane ring skeleton Raman modes observed in ordered and disordered P3HT phases under resonant excitation open a way to estimate the degree of molecular order of P3HT in blend films in general. The more ordered P3HT phase can be identified by (a) a large shift to lower wavenumber in the C=C mode peak position, (b) a much narrower fwhm of the C=C mode, and (c) a larger intensity of the C−C mode with respect to the C=C mode. Using these characteristics, we quantify the degree of molecular order of P3HT in blend films and the change in this molecular order induced by thermal annealing.

Table 1 summarizes the peak position and fwhm of the C=C mode and the intensity of the C−C mode relative to that of the C=C mode ($I_{C-C}/I_{C=C}$) of the RRa-P3HT, RR-P3HT films and also nonannealed RR-P3HT:PCBM and annealed RR-P3HT:PCBM films under excitation of different wavelengths.

Molecular Order of P3HT in the Blend Films. We estimate the molecular order of the P3HT in the nonannealed and annealed RR-P3HT:PCBM blend films relative to the limits of pristine ordered RR-P3HT and disordered RRa-P3HT films. Figure 4a shows the C=C mode of nonannealed RR-P3HT:PCBM blend film obtained under 488 nm excitation and a fit to this C=C peak constructed from the sum of spectra for the

Table 1. Summary of the Peak Position and fwhm of the C═C Mode and the Relative Intensity of the C−C Mode to the C═C Mode ($I_{C-C}/I_{C=C}$) for RRa-P3HT, RR-P3HT, RR-P3HT:PCBM, and Annealed RR-P3HT:PCBM Films under Different Excitation Wavelengths

λ_{EXC}	RRa-P3HT	RR-P3HT	RR-P3HT:PCBM	annealed RR-P3HT:PCBM
		Peak Position and (fwhm) of C═C Mode (cm^{-1})		
785 nm	1446 (109)	1446 (32)	1446 (39)	1446 (26)
633 nm	1450 (52)	1445 (24)	1445 (26)	1445 (23)
514 nm	1465 (39)	1450 (31)	1455 (39)	1449 (32)
488 nm	1470 (41)	1449 (32)	1460 (43)	1449 (33)
457 nm	1474 (43)	1451 (36)	1468 (45)	1449 (37)
		$I_{C-C}/I_{C=C}$		
633 nm	~0.10	~0.15	~0.15	~0.15
514 nm	~0.10	~0.14	~0.13	~0.14
488 nm	~0.09	~0.14	~0.12	~0.14
457 nm	~0.05	~0.12	~0.09	~0.12

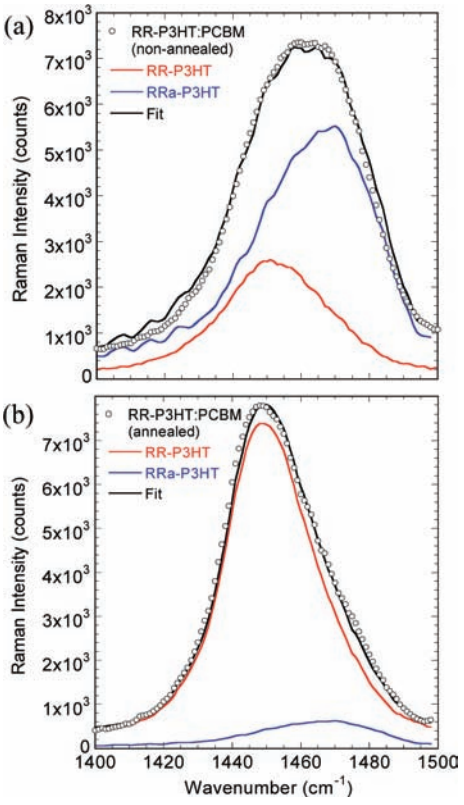

Figure 4. Raman spectra (C═C mode) of (a) nonannealed and (b) annealed RR-P3HT:PCBM films with the weighted Raman spectra of RR-P3HT and RRa-P3HT thin films used to fit the experimental spectra at 488 nm excitation.

C═C mode measured in ordered RR-P3HT and that for the C═C mode measured in disordered RRa-P3HT films, where the relative contribution of the two spectra is a fitting parameter. The composite spectrum obtained in this way produces a very good fit to the experimental C═C mode of the blend film when the ratio of contributions from disordered to ordered C═C mode spectra is 2.32 (calculated by using the integrated area of the C═C modes), thus indicating that the blend film is dominated by the disordered phase of P3HT.

To estimate the degree of molecular order of P3HT in RR-P3HT:PCBM blend films in a more quantitative way, it is necessary to determine the relative Raman scattering cross-section of the C═C mode of the ordered and disordered phases of P3HT under 488 nm excitation. The Raman scattering cross-section can be written by eq 1:[34]

$$P_R = P_0 \sigma D \, dz \tag{1}$$

in which P_R and P_0 are the scattered intensity in a given Raman line and the incident laser intensity with units of photons per second, σ is the Raman cross-section with unit of cm^2, D is the number density of scatters (molecules per cubic centimeter), and dz is the path length of the incident laser in the sample with unit of cm.

By using the relative values of P_0, D, dz, and P_R obtained (Supporting Information), the relative Raman scattering cross-section of the C═C mode ($\sigma_{RRa\text{-}P3HT}/\sigma_{RR\text{-}P3HT}$) in RRa-P3HT (disordered) to RR-P3HT (ordered) films under 488 nm excitation is approximated to be ~1.69. On the basis of this relative Raman scattering cross-section of the C═C mode of the ordered and disordered phases, we estimate the degree of molecular order of P3HT in the nonannealed RR-P3HT:PCBM blend film using the equation:

$$Cr_{/RR\text{-}P3HT}\ (\%) = \frac{P_{R(RR\text{-}P3HT)}}{P_{R(RR\text{-}P3HT)} + \dfrac{P_{R(RRa\text{-}P3HT)}}{\sigma_{RRa\text{-}P3HT}/\sigma_{RR\text{-}P3HT}}} \times 100 \tag{2}$$

in which $Cr_{/RR\text{-}P3HT}$ is the degree of order relative to a pristine RR-P3HT film. Using eq 2 with $P_{R(RRa\text{-}P3HT)}/P_{R(RR\text{-}P3HT)} \approx 2.32$, we estimate a content of ~42 ± 5% of ordered P3HT (RR-P3HT phase) in the nonannealed RR-P3HT:PCBM blend film. The associated error is calculated by averaging the obtained $Cr_{/RR\text{-}P3HT}$ values at various sample positions.

For the annealed RR-P3HT:PCBM film, the Raman spectrum of the C═C mode at 488 nm excitation is also fitted well with a sum of RRa-P3HT (disordered) and RR-P3HT (ordered) spectra (Figure 4b). The integrated area of the C═C mode of RRa-P3HT for the fit is ~0.10 relative to that of the RR-P3HT ($P_{R(RRa\text{-}P3HT)}/P_{R(RR\text{-}P3HT)} \approx 0.10$). From this, we estimate the degree of order of the P3HT in the annealed RR-P3HT:PCBM

dx.doi.org/10.1021/ja2013104 | J. Am. Chem. Soc. 2011, 133, 9834–9843

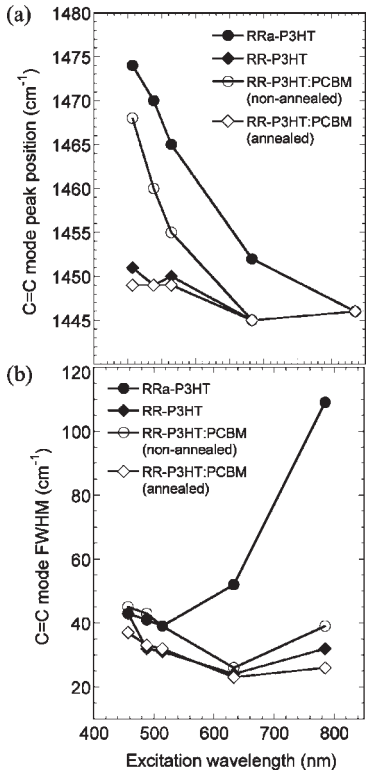

Figure 5. (a) Peak position and (b) fwhm of the C=C mode of RRa-P3HT, RR-P3HT, nonannealed RR-P3HT:PCBM, and annealed RR-P3HT:PCBM films at different excitation wavelengths.

blend film is ~94 ± 5% of that of RR-P3HT film. Note that the estimated values of degree of order in blend films do not correspond to a direct proportion of crystalline phase of P3HT in these blend films. Instead, they indicate the relative portion of ordered RR-P3HT phase in these blend films. Therefore, if RR-P3HT has ~15% of crystallinity in thin films,[35] then the nonannealed RR-P3HT:PCBM blend film has only ~6 ± 1% crystallinity of P3HT, and annealing of this blend film increases this value up to ~14 ± 1%. We also measured the Raman spectra (the C=C mode of P3HT) at the different homogeneous regions in the blend films, and our initial data indicate a similar degree of molecular order of P3HT in these regions.

Raman Spectra of Films at Different Excitation Wavelengths. Next, we investigate the effects of P3HT molecular order on the C=C mode peak position and its fwhm under different excitation wavelengths. Figure 5a shows the C=C mode peak position of RRa-P3HT and RR-P3HT films and nonannealed and annealed RR-P3HT:PCBM blend films at different excitation wavelengths (785, 633, 514, 488, and 457 nm). Table 1 summarizes the peak positions and fwhm of the C=C mode (and the intensity of the C−C mode relative to that of the C=C mode of the above films).

The peak position of the C=C mode shifts toward the higher wavenumber (higher energy) when the excitation wavelength gets shorter (higher energy). For RRa-P3HT film, this shift is strongest with the peak position of the C=C mode increasing from ~1446 cm^{-1} (785 nm excitation) to ~1450 cm^{-1} (633 nm excitation) to ~1465 cm^{-1} (514 nm excitation) to ~1470 cm^{-1} (488 nm excitation) to ~1474 cm^{-1} (457 nm excitation). In contrast, there is only a very small shift (~5 cm^{-1}) of this C=C mode peak position for RR-P3HT film.

Such a shift of the Raman peak position toward higher energy with higher excitation energy is termed "Raman dispersion". It has been reported that the degree of the Raman dispersion can have a large variation depending on the types of conjugated polymer, and some polymers even do not show any Raman dispersion.[36] For example, polyacetylene, polyenes, polypyrroles, and polyfurans show strong Raman dispersion, while polythiophene, polyfluorene, and poly(phenylene vinylenes) show no or very small Raman dispersion.[23,36,37] The different Raman dispersion behaviors of various conjugated polymers are still not well understood, and the origin of this dispersion is still under debate.

A number of different models such as the conjugation length model (CLM), the amplitude mode model (AMM), and the effective conjugation coordinate model (ECCM) have been suggested to explain the Raman dispersion phenomenon.[23,38−40] These models are all related to the (effective) conjugation length of a polymer. For example, in the CLM, a polymer is considered to be an infinite chain made up of segments of different conjugation lengths. These are distributed as Gaussian or bimodal functions and are treated as an ensemble of different chromophores. Under higher excitation energy, only the segments with shorter conjugation length (higher electronic transition) will be in resonance with excitation energy, leading to the Raman peak at higher wavenumber.[41,42] In the AMM, the different degree of electron−phonon coupling of a polymer under a particular excitation is considered using an effective electron−phonon coupling parameter. This parameter strongly depends on the conjugation length, with shorter conjugation length leading to larger electron−phonon coupling.[41,43] Finally, the ECCM focuses on a Raman mode, which distorts the molecule from the aromatic to quinoid valence form. Such a mode is strongly in resonance with a particular excitation energy and thus dominates the resonant Raman spectrum.[41,44] As the conjugation length of a polymer increases, the force constant originating from the interaction between the central unit and the units at a distance s from the central one along the one-dimensional lattice increases.[36] This force constant reduces the total force constant, causing the Raman mode to be downshifted in wavenumber with increasing conjugation length. All of these three models can explain the Raman dispersion behavior of the RRa-P3HT and RR-P3HT films observed here.

Coming back to our P3HT system, we observed interesting trends of the Raman shift in blend films (Figure 5a). For nonannealed RR-P3HT:PCBM blend films, the trend of such a shift of the C=C mode peak position to higher wavenumber with excitation wavelength is very similar to that found in RRa-P3HT film, that is, a large shift to higher wavenumber (>20 cm^{-1}) as the excitation wavelength gets shorter. However, this trend changes and becomes more similar to that found in RR-P3HT film when the blend film is annealed, that is, a very small shift to higher wavenumber (<5 cm^{-1}) with shorter excitation wavelengths. A large Raman dispersion of the C=C mode in the nonannealed RR-P3HT:PCBM blend film can be understood by considering more mixture of disordered and ordered P3HT phases in this film. A selective excitation of different phases is possible, that is, being able to selectively excite the more disordered phase (shorter conjugation length) with shorter wavelength, and thus the peak position of the C=C mode appears at a higher wavenumber (analogous to that of RRa-P3HT film). After annealing this RR-P3HT:PCBM blend film, there is a change in P3HT phase from disordered to a more

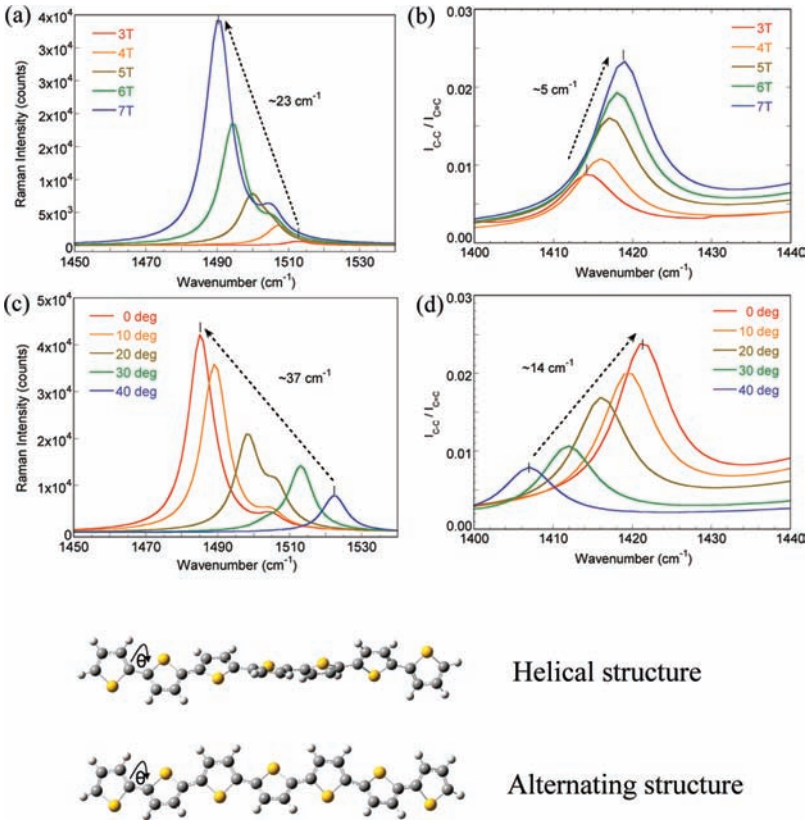

Figure 6. Helical and alternating structures of the 7-unit thiophene oligomer (bottom). Calculated Raman spectra of 3−7 thiophene units, (a) C═C mode and (b) magnitude of the C−C mode relative to the C═C mode. Calculated Raman spectra of 7 thiophene units with 0−40° dihedral angles (helical chain conformation), (c) C═C mode and (d) magnitude of C−C mode relative to the C═C mode.

ordered state with a degree of molecular order similar to that found in the RR-P3HT film, therefore producing a Raman dispersion behavior similar to that of the RR-P3HT film. Note that there is a larger Raman shift of the C═C mode of P3HT (when comparing the nonannealed blend film with the annealed blend film) as the excitation wavelength gets shorter ($\Delta\nu$ = ~6 cm^{-1} at 514 nm; ~11 cm^{-1} at 488 nm; ~19 cm^{-1} at 457 nm), indicating the stronger detection of disordered phase of P3HT at higher excitation energy. Therefore, we can tune the excitation energy to monitor the different phases of P3HT in various thin films.

Figure 5b shows the fwhm of the C═C mode at different excitation wavelengths. The change in fwhm of the C═C mode with excitation wavelengths for the nonannealed RR-P3HT:PCBM and annealed RR-P3HT:PCBM blend films is also similar to that of RRa-P3HT and RR-P3HT films, respectively. These results are in good agreement with the phase change of P3HT molecules from a more disordered to a more ordered state in the RR-P3HT:PCBM blend film upon thermal annealing. Finally, we notice that enhancement of the Raman intensity of the two main in-plane ring skeleton modes (C═C and intraring C−C stretching modes) is about a factor of 2 larger than the lower frequency side-chain modes under resonant excitations (data not shown).

Raman Simulations. To understand more about the behavior of the P3HT C═C and C−C modes in ordered and disordered phases and its behavior with excitation wavelength, we performed two series of Raman simulations. First, Raman spectra were calculated for a series of thiophene oligomers containing 3 to 7 units to study the effect of increasing chain length on the properties of the C═C and C−C stretch modes. Second, to study the effect of conjugated backbone planarity on the C═C and C−C modes, Raman spectra were calculated for a 7-unit thiophene chain with varying dihedral angles from 40° to 0° in both helical and alternating structures (Figure 6).

Figure 6a shows the calculated C═C mode of 3−7 thiophene units. Our calculated spectra are similar to those reported by Milani et al.[38] The peak positions of the C═C and C−C modes are 1490 and 1419 cm^{-1} (seven thiophene units), respectively. With an empirical scaling factor of 0.97,[45] the positions of the C═C and C−C modes become 1449 and 1379 cm^{-1}, in good agreement with the experimental values. The peak position of the C═C mode shifts to lower wavenumber significantly (~23 cm^{-1}) when increasing the chain length from 3 to 7 units. This result indicates that the C═C mode shifts to lower wavenumber for molecules containing longer conjugation segments. According to this simulation, our observation that the Raman C═C mode of RR-P3HT film lies at lower wavenumber than that of RRa-P3HT film implies that RR-P3HT backbone contains longer conjugated segments than that of RRa-P3HT. This is reasonable as RR-P3HT is known to be more ordered, implying longer conjugated segments than in its disordered form.

The calculated intensity of the C−C mode relative to the C═C mode ($I_{C-C}/I_{C=C}$) increases from ~0.01 to ~0.03 with increasing chain length, without significant changes in the peak position (only 5 cm^{-1} when going from 3 to 7 thiophene units) (Figure 6b). This result suggests that a molecule with a longer conjugation segment has a larger relative C−C mode intensity as

dx.doi.org/10.1021/ja2013104 |J. Am. Chem. Soc. 2011, 133, 9834–9843

compared to a molecule with a shorter conjugation segment, while having similar C−C peak positions. Such an increase in the relative C−C mode intensity might be related to better electron−phonon coupling of this mode and/or increased charge transfer from C═C bonds as suggested for oligothiophenes.[46] Our calculated results are consistent with the experimental results showing that the relative intensity of the C−C mode of RR-P3HT film is larger than that of RRa-P3HT film and both have similar C−C peak positions.

Figure 6c shows the calculated C═C mode of a 7-unit long thiophene oligomer with dihedral angles varying from 40° to 0°. We notice that as the molecule becomes more planar, the peak position of the C═C mode shifted to lower wavenumber (∼37 cm^{-1} shift when going from 40° to 0°). Therefore, our observation of the C═C mode of RR-P3HT film at a lower wavenumber than RRa-P3HT film is consistent with a more planar backbone conformation in RR-P3HT, which leads to better ordering of RR-P3HT molecules.

The intensity of the C−C mode relative to the C═C mode also increases with more planar backbone conformation (Figure 6d). The peak position of the C−C mode shifts considerably to higher wavenumber with more planar conformation (∼14 cm^{-1} shift when going from 40° to 0°). This is in contrast to the peak position of the C−C mode experimentally measured, which is insensitive to molecular order. However, we note that the difference in dihedral angles between the ordered and disordered phases may not be as large as 40°. Our simulations may therefore also imply that the ordered phase of the P3HT molecule has a more planar chain conformation than its disordered phase. This is reasonable as a more planar backbone conformation favors the well-ordered lamellar packing of RR-P3HT molecules.[1] Similarly, these concepts of longer conjugation segment or/and more planar chain conformation can be used to explain the behavior of the C═C and C−C modes when RR-P3HT:PCBM is annealed (i.e., a phase change of P3HT from disordered to more ordered form). The Raman spectra calculated (both C═C and C−C modes) using the alternating chain structure are similar to those using the helical chain structure.

A large Raman dispersion (shift of the C═C mode peak position to higher wavenumber with higher excitation energy) observed in the RRa-P3HT film can also be explained with our simulations. With higher excitation energy, the shorter conjugated segments (absorbing at higher energy) of the polymers are now more in resonance. This is analogous to less conjugated conformation, which has a peak position of the C═C mode at higher wavenumber. On the contrary, the insensitivity of the C═C mode peak position observed in the RR-P3HT film with excitation energy may imply that there is a relatively lower density of short conjugation segments in these polymers.

Device Performance. Figure 7 shows the current density (J)−voltage (V) characteristics of RRa-P3HT:PCBM, annealed RRa-P3HT:PCBM, RR-P3HT:PCBM, and annealed RR-P3HT:PCBM solar cells measured under AM 1.5 condition at 100 mW/cm^2. Table 2 summarizes the device parameters of the corresponding solar cells. The short-circuit current density (J_{SC}) values of RRa-P3HT:PCBM and annealed RRa-P3HT:PCBM devices are the same, and they are significantly smaller than that of the RR-P3HT:PCBM device. This is consistent with the considerable amount of ordered phase of P3HT that already existed in the RR-P3HT:PCBM film from our Raman data. The J_{SC} of RR-P3HT:PCBM solar cell after annealing is significantly increased, which is also consistent with the increase of ordered phases of P3HT after thermal annealing from our Raman data.

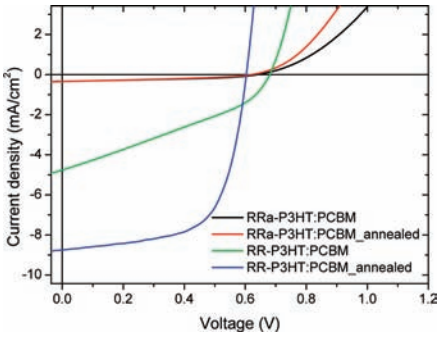

Figure 7. $J-V$ curves of RRa-P3HT:PCBM, annealed RRa-P3HT:PCBM, RR-P3HT:PCBM, and annealed RR-P3HT:PCBM solar cells measured under AM 1.5 condition at 100 mW/cm^2.

Table 2. Summary of Device Parameters (V_{OC}, Open Circuit Voltage; J_{SC}, Short Circuit Current Density; FF, Fill Factor; PCE, Power Conversion Efficiency) of RRa-P3HT:PCBM, Annealed RRa-P3HT:PCBM, RR-P3HT:PCBM, and Annealed RR-P3HT:PCBM Solar Cells Measured under AM 1.5 Condition at 100 mW/cm^2

	RRa-P3HT:PCBM	annealed RRa-P3HT:PCBM	RR-P3HT:PCBM	annealed RR-P3HT:PCBM
V_{OC} (V)	0.64	0.62	0.68	0.60
J_{SC} (mA/cm^2)	−0.34	−0.34	−4.79	−8.72
FF	0.39	0.36	0.33	0.64
PCE (%)	0.09	0.08	1.07	3.39

CONCLUSIONS

We have presented strong experimental evidence that the behavior of the C═C and C−C Raman modes of RR-P3HT in blend films with PCBM, both before and after thermal annealing and over a wide range of excitation wavelengths, can be explained in terms of contributions from the ordered and disordered phases of P3HT. The C═C mode can be treated simply as a superposition of the modes characteristic of the two different phases, which can be easily distinguished under resonant excitation conditions. This observation leads to a simple method to quantify the degree of order of RR-P3HT molecules in the blend films. We estimated the degree of molecular order of P3HT in the RR-P3HT:PCBM blend films before and after thermal annealing to be ∼42 ± 5% and ∼94 ± 5% of that of pristine RR-P3HT film, respectively. Together with Raman simulations, we explain the behavior of the C═C mode (including peak position and Raman dispersion) of P3HT in terms of its conjugation length and chain conformation. The Raman simulations suggest that RR-P3HT (ordered phase) has a longer conjugated length with planar chain conformation than that of RRa-P3HT (disordered phase), which is consistent with a higher degree of molecular ordering in RR-P3HT. The degree of molecular order of P3HT in the blend films is well correlated with the performance of the corresponding solar cells. Our results demonstrate that Raman spectroscopy under resonant excitations is a simple, but very powerful technique to study the molecular order of conjugated polymers in their blend films.

■ ASSOCIATED CONTENT

Supporting Information. (1) Methodology used to estimate the relative Raman scattering cross-section of the C═C mode of ordered and disordered P3HT phases, (2) absorption spectra of RRa-P3HT and RR-P3HT films before and after annealing, and (3) examples of the Raman spectra prior to subtractions of background signals. This material is available free of charge via the Internet at http://pubs.acs.org.

■ AUTHOR INFORMATION

Corresponding Authors
ji-seon.kim@imperial.ac.uk; craig.murphy@npl.co.uk.

■ ACKNOWLEDGMENT

This work is funded by the EPSRC-NPL Post-Doctoral Research Partnership (EP/G062056/1), the SUPERGEN Excitonic Solar Cell Consortium Grant (EP/G031088/1) and the World Class University (WCU) Program in Korea (Grant No. R32-10051).

■ REFERENCES

(1) Yamamoto, T.; Komarudin, D.; Arai, M.; Lee, B. L.; Suganuma, H.; Asakawa, N.; Inoue, Y.; Kubota, K.; Sasaki, S.; Fukuda, T.; Matsuda, H. *J. Am. Chem. Soc.* **1998**, *120*, 2047–2058.
(2) Brown, P. J.; Thomas, D. S.; Kohler, A.; Wilson, J. S.; Kim, J. S.; Ramsdale, C. M.; Sirringhaus, H.; Friend, R. H. *Phys. Rev. B* **2003**, *67*, 064203.
(3) Pandey, S. S.; Takashima, W.; Nagamatsu, S.; Endo, T.; Rikukawa, M.; Kaneto, K. *Jpn. J. Appl. Phys., Part 2* **2000**, *39*, L94–L97.
(4) Sirringhaus, H.; Brown, P. J.; Friend, R. H.; Nielsen, M. M.; Bechgaard, K.; Langeveld-Voss, B. M. W.; Spiering, A. J. H.; Janssen, R. A. J.; Meijer, E. W.; Herwig, P.; de Leeuw, D. M. *Nature* **1999**, *401*, 685–688.
(5) Gunes, S.; Neugebauer, H.; Sariciftci, N. S. *Chem. Rev.* **2007**, *107*, 1324–1338.
(6) Li, G.; Shrotriya, V.; Huang, J. S.; Yao, Y.; Moriarty, T.; Emery, K.; Yang, Y. *Nat. Mater.* **2005**, *4*, 864–868.
(7) Kim, Y.; Cook, S.; Tuladhar, S. M.; Choulis, S. A.; Nelson, J.; Durrant, J. R.; Bradley, D. D. C.; Giles, M.; McCulloch, I.; Ha, C. S.; Ree, M. *Nat. Mater.* **2006**, *5*, 197–203.
(8) Padinger, F.; Rittberger, R. S.; Sariciftci, N. S. *Adv. Funct. Mater.* **2003**, *13*, 85–88.
(9) Chirvase, D.; Parisi, J.; Hummelen, J. C.; Dyakonov, V. *Nanotechnology* **2004**, *15*, 1317–1323.
(10) Mihailetchi, V. D.; Xie, H. X.; de Boer, B.; Koster, L. J. A.; Blom, P. W. M. *Adv. Funct. Mater.* **2006**, *16*, 699–708.
(11) Honea, E. C.; Ogura, A.; Murray, C. A.; Raghavachari, K.; Sprenger, Wo.; Jarrold, M. F.; Brown, W. L. *Nature* **1993**, *366*, 42–44.
(12) Donley, C. L.; Zaumseil, J.; Andreasen, J. W.; Nielsen, M. M.; Sirringhaus, H.; Friend, R. H.; Kim, J. S. *J. Am. Chem. Soc.* **2005**, *127*, 12890–12899.
(13) Schmidtke, J. P.; Kim, J. S.; Gierschner, J.; Silva, C.; Friend, R. H. *Phys. Rev. Lett.* **2007**, *99*, 167401.
(14) Kneipp, K.; Wang, Y.; Kneipp, H.; Perelman, L. T.; Itzkan, I.; Dasari, R.; Feld, M. S. *Phys. Rev. Lett.* **1997**, *78*, 1667–1670.
(15) Walter, M. J.; Lupton, J. M.; Becker, K.; Feldmann, J.; Gaefke, G.; Hoger, S. *Phys. Rev. Lett.* **2007**, *98*, 137401.
(16) Steidtner, J.; Pettinger, B. *Phys. Rev. Lett.* **2008**, *100*, 236101.
(17) Wang, X.; Zhang, D.; Braun, K.; Egelhaaf, H. J.; Brabec, C. J.; Meixner, A. J. *Adv. Funct. Mater.* **2010**, *20*, 492–499.
(18) Kim, J. S.; Ho, P. K. H.; Murphy, C. E.; Baynes, N.; Friend, R. H. *Adv. Mater.* **2002**, *14*, 206–209.
(19) Kim, J. S.; Ho, P. K. H.; Murphy, C. E.; Seeley, A. J. A. B.; Grizzi, I.; Burroughes, J. H.; Friend, R. H. *Chem. Phys. Lett.* **2004**, *386*, 2–7.
(20) Kim, J. S.; Ho, P. K. H.; Murphy, C. E.; Friend, R. H. *Macromolecules* **2004**, *37*, 2861–2871.
(21) Soltzberg, L. J.; Slinker, J. D.; Flores-Torres, S.; Bernards, D. A.; Malliaras, G. G.; Abruna, H. D.; Kim, J. S.; Friend, R. H.; Kaplan, M. D.; Goldberg, V. *J. Am. Chem. Soc.* **2006**, *128*, 7761–7764.
(22) Ferraro, J. R.; Nakamoto, K. *Introductory Raman Spectroscopy*; Academic Press: San Diego, CA, 1994.
(23) Yacoby, Y.; Ehrenfreund, E. In *Light Scattering in Solids VI*; Cardona, M., Gfintherodt, G., Eds.; Springer: Berlin/Heidelberg, 1991; Vol. 68, p 73.
(24) Miller, S.; Fanchini, G.; Lin, Y.-Y.; Li, C.; Chen, C.-W.; Su, W.-F.; Chhowalla, M. *J. Mater. Chem.* **2008**, *18*, 306–312.
(25) Yun, J.-J.; Peet, J.; Cho, N.-S.; Bazan, G. C.; Lee, S. J.; Moskovits, M. *Appl. Phys. Lett.* **2008**, *92*, 251912.
(26) Gao, Y.; Gery, J. K. *J. Am. Chem. Soc.* **2009**, *131*, 9654–9662.
(27) Janssen, G.; Aguirre, A.; Goovaerts, E.; Vanlaeke, P.; Poortmans, J.; Manca *J. Eur. Phys. J. Appl. Phys.* **2007**, *37*, 287–290.
(28) Frisch, M. J.; et al. *Gaussian 09*, revision A.02; Gaussian, Inc.: Wallingford, CT, 2009.
(29) Van Eijck, L.; Johnson, M. R.; Kearly, G. J. *J. Phys. Chem. A* **2003**, *107*, 8980–8984.
(30) Campoy-Quiles, M.; Kanai, Y.; El-Basaty, A.; Sakai, H.; Murata, H. *Org. Electron.* **2009**, *10*, 1120–1132.
(31) Baibarac, M.; Lapkowski, M.; Pron, A.; Lefrant, S.; Baltog, I. *J. Raman Spectrosc.* **1998**, *29*, 825–832.
(32) Ballantyne, A. M.; Ferenczi, T. A. M.; Campoy-Quiles, M.; Clarke, T. M.; Maurano, A.; Wong, K. H.; Zhang, W. M.; Stingelin-Stutzmann, N.; Kim, J. S.; Bradley, D. D. C.; Durrant, J. R.; McCulloch, I.; Heeney, M.; Nelson, J.; Tierney, S.; Duffy, W.; Mueller, C.; Smith, P. *Macromolecules* **2010**, *43*, 1169–1174.
(33) Van Bavel, S. S.; Sourty, E.; de With, G.; Loos, J. *Nano Lett.* **2009**, *9*, 507–513.
(34) McCreery, R. L. *Raman Spectroscopy for Chemical Analysis*; John Wiley & Sons Inc.: New York, 2000.
(35) Malik, S.; Nandi, A. K. *J. Polym. Sci., Part B: Polym. Phys.* **2002**, *40*, 2073–2085.
(36) Hernandez, V.; Castiglioni, C.; Del Zoppo, M.; Zerbi, G. *Phys. Rev. B* **1994**, *50*, 9815–9823.
(37) Tsoi, W. C.; Lidzey, D. G. *J. Phys.: Condens. Matter* **2008**, *20*, 125213.
(38) Milani, A.; Brambilla, L.; Del Zoppo, M.; Zerbi, G. *J. Phys. Chem. B* **2007**, *111*, 1271–1276.
(39) Millen, R. P.; de Faria, D. L.; Temperini, M. L. A. *Quim. Nova* **2005**, *28*, 289–295.
(40) Ozaki, M.; Ehrenfreund, E.; Benner, R. E.; Barton, T. J.; Yoshino, K.; Vardeny, Z. V. *Phys. Rev. Lett.* **1997**, *79*, 1762–1765.
(41) Jadamiec, M.; Lapkowski, M.; Officer, D. L.; Wagner, P.; Gordon, K. C. *Int. J. Nanotechnol.* **2009**, *6*, 344–354.
(42) Brivio, G. P.; Mulazzi, E. *Phys. Rev. B* **1984**, *30*, 876–882.
(43) Horovitz, B. *Solid State Commun.* **1982**, *41*, 729–734.
(44) Castiglioni, C.; Navarrete, J. L. T.; Zerbi, G.; Gussoni, M. *Solid State Commun.* **1988**, *65*, 625–630.
(45) Scott, A. P.; Radom, L. *J. Phys. Chem.* **1996**, *100*, 16502–16513.
(46) Louarn, G.; Buisson, J. P.; Sefrant, S.; Fichou, D. *J. Phys. Chem.* **1995**, *99*, 11399–11404.